Synchronizing gas injections and time-resolved data acquisition for perturbation-enhanced APXPS experiments.

Evgeniy A. Redekop[1,†,*], Niclas Johansson[2,†], Esko Kokkonen[2], Samuli Urpelainen[3], Felipe Lopes da Silva[2,3,4,5], Mikko Kaipio[6], Heta-Elisa Nieminen[6], Foqia Rehman[5], Ville Miikkulainen[6,**],Mikko Ritala[6], and Unni Olsbye[1]

[1] – Centre for Materials Science and Nanotechnology (SMN), Department of Chemistry, University of Oslo, Oslo 0371, Norway

[2] – MAX IV Laboratory, Lund University, SE-221 00 Lund, Sweden

[3] – Nano and Molecular Systems Research Unit, University of Oulu, FI-90014 Oulu, Finland

[4] – Environmental and Chemical Engineering Research Unit, University of Oulu, FI-90014 Oulu, Finland

[5] – Department of Physics, Lund University, SE-221 00 Lund, Sweden

[6] – Department of Chemistry, University of Helsinki, FI-00014 Helsinki, Finland

[†] - authors contributed equally

[*] - corresponding author, evgeniyr@smn.uio.no

** - current affiliation: Department of Chemistry and Materials Science, Aalto University, FI-00076 Aalto, Finland

Abstract

An experimental approach is described in which well-defined perturbations of the gas feed into an Ambient Pressure X-Ray Photoelectron Spectroscopy (APXPS) cell are fully synchronized with the time-resolved XPS data acquisition. These experiments unlock new possibilities for investigating the properties of materials and chemical reactions mediated by their surfaces, such as those in heterogeneous catalysis, surface science, and coating/deposition applications. Implementation of this approach, which is termed perturbation-enhanced APXPS, at the SPECIES beamline of MAX IV Laboratory is discussed along with several experimental examples including individual pulses of N_2 gas over Au foil, a multi-pulse titration of oxygen vacancies in a pre-reduced TiO_2 single crystal with O_2 gas, and a sequence of alternating precursor pulses for Atomic Layer Deposition (ALD) of TiO_2 on a silicon wafer substrate.

1. Introduction

Exposure of solid surfaces to gaseous environments is an essential part of experimental studies in many disciplines including surface science, heterogeneous catalysis, materials science, or heterogeneous chemistry of aerosols. Gas treatments are used, for example, to remove surface contaminants, to alter the chemical composition of surfaces and/or adsorbed layers, grow thin films, and, importantly, to perform surface-mediated (catalytic) chemical reactions. Exposure to gaseous stimuli can also be used to elicit various responses in the bulk of certain materials through electronic (current), mass (diffusion), or other forms of transport processes, which is relevant in sensing and energy conversion applications. Therefore, it is highly desirable to be able to exert precise control over the amount and temporal modality of gas exposure in combination with spectroscopic and structural characterization tools employed in fundamental studies of various materials. Experiments with well-defined transient perturbations (pulse, step, and periodic wave) are especially valuable, as they deliver more quantifiable real-time data about physico-chemical processes investigated.

In chemical kinetics, transient gas perturbations are routinely employed to investigate the reaction mechanisms and derive the intrinsic reaction parameters of gas-surface interactions[1–3]. For example, step perturbations in the isotopic composition of the feed are used in Steady-State Isotopic Transient Kinetic Analysis (SSITKA) to evaluate the mean surface residence times and abundances of reaction intermediates[4–6]. Concentration step-transients under flow conditions are widely used for kinetic investigations[7]. Periodic (pressure) waves are used in frequency methods to scrutinize the reaction kinetics under such operating conditions that may not be accessible to other transient methods[8,9]. Transient perturbations of the gas composition are also utilized in many spectroscopic and structural methods, e.g. refs. [10–12], especially to enhance the sensitivity to such reaction intermediates that have their signals obscured by spectator species[13–15].

This work derives motivation from Temporal Analysis of Products (TAP) – a powerful transient technique for precise kinetic characterization of complex catalytic materials and reactions[16,17]. TAP employs nanomolar pulses of reactants that are injected over an evacuated sample (packed bed configuration) to probe its kinetic properties. Time-resolved (in the range of 1ms) Quadrupole Mass-Spectrometry (QMS) responses of gaseous species are quantitatively analyzed, primarily within the model of Knudsen diffusion[18], to extract a rich variety of intrinsic kinetic characteristics. Well-defined gas perturbations (pulses) also allow for superior control over the chemical status of the catalyst surface[16,17,19,20]. When complemented by surface spectroscopy measurements on a comparable time-scale, such pulse-response experiments can have profound implications for mechanistic studies in catalysis and materials science. For example, complementary spectro-kinetic data can be assimilated in a unified modeling framework, such as mean-field microkinetics or the Rate-Reactivity Model (RRM)[21], which improves our fundamental understanding of complex surfaces. Implementation of such perturbation-enhanced experiments in conjunction with surface-sensitive electron spectroscopies is particularly desirable for investigating correlations between the electronic structure and kinetic properties of materials[22]. However, this pursuit faces a number of technical and methodological challenges.

X-Ray (XPS) and Ultraviolet (UPS) Photoelectron Spectroscopies are essential surface-sensitive techniques that are widely applied for materials characterization. Historically, Molecular Beam Scattering (MBS) methodology was utilized in conjunction with XPS as well as Infrared (IR) and Electron Energy Loss (EELS) spectroscopy measurements in surface science as a mean to impose a well-defined gas perturbation, whereby the probe molecules are delivered onto a sample surface by a focused molecular beam source in a continuous or periodic manner[23,24]. From the kinetics point of view, MBS experiments derive their strength from the well-defined, single-collision mode of gas transport in the free molecular flow regime, which facilitates quantitatively accurate estimations of intrinsic kinetic parameters from the time-resolved mass-spectrometric and spectroscopic signals[25–27]. When molecular beams are employed, gaseous species can be quantitatively monitored by a mass-spectrometer in addition to monitoring surface species with spectroscopy. These combined spectro-kinetic data can be very informative for elucidating the reaction mechanisms on well-defined model surfaces, such as single crystals or thin films. However, MBS-enhanced spectroscopic experiments on model surfaces are limited in scope when it comes to investigating more structurally complex materials under technologically relevant operating conditions (e.g. higher pressure). Moreover, molecular beam sources and mass-spectrometers are rarely installed in the vicinity of the sample in conventional (commercial) XPS systems due to additional technical complexities. As a result, most surface spectroscopies are performed in high vacuum or in a static gas environment inside "back-filled" vacuum chambers. One notable example to the contrary is the Dynamic High Pressure (DHP) approach developed at Elettra synchrotron[28], in which gaseous pulse transients are employed to augment conventional XPS measurements. DHP utilizes short, intense pulses of gas to briefly expose the sample surface to elevated pressures of gaseous reactants. Although it may not be possible to acquire XPS spectra while such a pulse is in progress, they can readily be acquired in between the pulses to monitor the evolution of the surface within a series of pulses or to monitor the reactions of relatively long-lived adsorbents that remain on the surface immediately after a pulse.

Over the course of recent decades, a number of methodological and instrumentation advancements have opened new possibilities for *in situ* XPS investigations of chemically-reactive surfaces, as recently reviewed by Schnadt et al.[29] Ambient Pressure XPS (APXPS) instruments (e.g. see [30–32] and references therein) have become a commonplace at large synchrotron radiation facilities and, increasingly, in many home laboratories[33]. These instruments allow for the gas pressure in the vicinity of the sample surface to be increased up to 50-100 mbar, while still providing XPS spectra of high quality. This is achieved by placing a very narrow (100-1000 μm diameter) aperture of a differentially-pumped electron analyzer only one or two aperture diameters away from the sample surface in order to minimize the escape path of the photoelectrons through the gas layer, while maintaining elevated pressure of reactants at the sample surface. Subsequently developed small dead volume cells[34,35] feature a more rapid gas exchange within the cell volume – an essential pre-requisite for kinetically well-defined *in situ* APXPS experiments. The cutting edge APXPS cells with unique geometries[36] or capped with graphene membranes[37,38] achieve unprecedented high pressures up to several bars. Furthermore, highly-sensitive detectors such as Delay Line Detectors (DLD)[39,40] provide sufficient signal-to-noise ratio for acquiring XPS spectra on the sub-second time scale. Other factors contributing to the improved data quality and temporal resolution include the high brilliance of synchrotron radiation and the high transmission of electron analyzers. Valuable kinetic insights about surface reactions have been gained by temperature-programmed APXPS measurements. [41] The aforementioned technological developments in photoelectron spectroscopies can potentially offer unprecedented experimental capabilities whereby well-defined perturbations of the surrounding gas composition can be delivered to model as well as complex materials, while their surfaces are simultaneously monitored by real-time XPS. We refer to this mode of experimentation as *perturbation-enhanced APXPS*, and the first examples of such experiments have already appeared for powdered catalysts in the recent literature[42].

One of the practical challenges in conducting perturbation-enhanced XPS measurements is the synchronization of electronic components for precise gas control and data acquisition, which is

crucial for achieving accurate temporal alignment of the resulting datasets and implementing advanced automation. We foresee that such a precise synchronization will become increasingly important for kinetically well-defined, TAP-like APXPS measurements. Here we report the development of a hardware/software interface for performing well-defined, fully automated gas perturbations that are synchronized with the time-resolved XPS data acquisition. Selected experimental case studies are described to illustrate the potential application scope of these novel capabilities in materials research, evaluate their limits in the context of the state-of-the-art APXPS instruments, and discern the directions in which further developments could be fruitful.

2. Implementation

Experiments were developed at the APXPS end station of the SPECIES beamline[43,44] at MAX IV Laboratory. The endstation[35] is equipped with an ambient pressure XPS cell, a differentially pumped electron analyzer (SPECS Phoibos 150 NAP), and a DLD detector from Surface Concept. An Al/Si_3N_4 window mounted on the cell allows the X-rays (either from an anode source or the synchrotron) to enter the cell without compromising the high vacuum conditions of the beamline and the rest of the vacuum system. The main aim of this work was to extend the capabilities of the instrument to enable simultaneous triggering (i.e. in the same time frame) of the gas perturbation by an arbitrary injection device placed upstream of the AP cell and the XPS data acquisition by the spectrometer.

2.1. Hardware

Different components of the system are schematically depicted in Figure 1 and include (1) a synchronizing controller interfaced with (2) an injection device and (3) DLD. RaspberryPi 3 unit (RPi)[45] which runs the Raspbian operating system was selected as the core of the system. RPi have many advantages in the context of this application, such as a low price and compact dimensions, but

the most important feature is its fully integrated general-purpose input/output (GPIO) circuit which allows the RPi to easily interface with external equipment (see the circuit in Supplementary Note 1).

Gases are supplied into the AP cell (inner volume ca. 200 ml) via two ca. 2 m long inlet lines (4 mm ID), both of which open into the conically-shaped annulus surrounding the nozzle of the electron analyzer in order to deliver gas in close proximity of the sample surface. Pneumatically actuated diaphragm-sealed valves from Swagelok (model 6LVV-DPS4-C) were used as gas injectors upstream of the inlet lines, and their actuation was synchronized with the DLD data acquisition. Gases were evacuated from the back of the AP cell volume through a ca. 2 m long outlet line (4 mm ID) by a turbo-molecular pump (pumping speed 67 $L \cdot s^{-1}$). The composition of the outlet gas stream was measured at the end of the outlet line by a Quadrupole Mass-Spectrometer (QMS) via a variable leak valve. In order to control pressure inside the AP cell (measured by a Ceravac CTR 100 N capacitance pressure gauge at the outlet line, approximately 2 m from the cell and before the QMS entrance), a variable leak valve was placed upstream of the pneumatic valves. The leak rate was adjusted in advance to achieve the desired pressure in the cell and later kept at this constant opening during the experiment. The two pneumatic valves were operated in a dual mode with two configurations (see Figure 2): (a) the inlet valve open and the bypass valve closed which allows for gas injection into the AP cell and (b) the inlet valve closed and the bypass valve open which creates a gas-flow to the outlet pump and ensures no pressure build-up in the line. The bypass line was connected to the gas evacuation line of the APXPS end station pumped by a turbo-molecular pump. The trigger signal was level-shifted to 24V by relays to operate the pneumatic valve actuators (shown in the upper right corner of Supplementary Figure S1b), which were in turn controlled by the RPi.

2.2. Software

The control software was written in Python which offers a wide variety of libraries for, among other things, the control of the RPi's GPIO circuit and user interfaces[45,46]. Python software was developed to (1) implement the gas injection sequences by triggering the pneumatic valves and

(2) initiate the data acquisition by triggering the DLD detector. Some of the data acquisition parameters, such as the pass energy of the analyser, are determined by the voltages applied to the spectrometer, which are set externally by the SpecsLab Prodigy software. The acquisition of the electron spectra by the DLD, on the other hand, was controlled by a software provided by the Surface Concept GmbH. This data acquisition software records individual "snapshots" of the detector image when provided by an external trigger signal, which here was generated by the RPi. The acquired images are converted into spectra by integrating over the non-dispersive (non-energy) axis. The energy scale is calibrated in a separate experiment with synchrotron light by measuring a known photoelectron line at different positions on the detector by changing the incident photon energy. This enables the calibration of the detector energy scale. Finally, the acquired APXPS spectra are aligned to the gas injection sequences in time by the time stamps in the data files.

3. Examples of application in APXPS experiments

The newly developed hardware/software interface was tested in three types of experiments, all of which have a potential to significantly enhance the studies of reactive materials at the SPECIES beamline: (1) pulse-response real-time analysis of gas and surface species, (2) pulsed titration of surface species for step-wise alteration of the surface composition, and (3) cycled exposure of surfaces to the Atomic Layer Deposition (ALD) precursors. Experiments were conducted in the "off-line" mode with a Mg Kα X-Ray source (SPECS XR50, 1253.6 eV, 250W) which can be used in addition to synchrotron light at the APXPS endstation.

3.1. Time-resolved monitoring of gas and surface species

Monitoring the sample surface with XPS in real-time in response to a transient change of the gas composition is of great interest for applications in catalysis and surface chemistry. To demonstrate the perturbation-enhanced time-resolved data acquisition mode, nitrogen gas was injected over the gold foil, while XPS signals at N 1s and Au 4f binding energies were monitored as

functions of time (see Figure 3). Nitrogen gas does not react with gold under these conditions, making their combination a convenient model for elucidating the temporal characteristics of the signal in the absence of chemical reactions. The beginning of the injected square pulse (see Figure 3(a)) defined the origin of the time axis (t=0) for the DLD detector. The QMS located downstream (outlet line) from the AP cell was operated in a continuous data acquisition mode, and the QMS data were aligned with the DLD time line post factum, based on the time stamps in the data files. The valve opening time (or pulse duration) t_v served as the control parameter regulating pulse intensity. The pressure in the AP cell was adjusted using the variable leak valve to 1 mbar with the pulse valve fully open.

XPS responses of nitrogen gas (N 1s) above the sample surface and of gold foil (Au 4f) are shown in Figures 3(b) and 3(c), respectively. These data were recorded at 100 eV analyser pass energy, 3mm slit width, and 100 ms dwell time for each DLD image. Raw images (see example in Supplementary Note 2) were summed over all channels to produce time-resolved signals. Transient changes in both N 1s and Au 4f signals are distinguishable from the background already for the 1 s valve opening time, albeit with low signal-to-noise ratio, and they become significantly more prominent for a longer valve opening. The inverted shape of the pulse in the Au 4f signal is due to the increased attenuation of photoelectrons from the surface by the injected N_2 gas molecules. Both N 1s and Au 4f signals in these figures were binned to the time resolution of 300 ms in order to improve the signal-to-noise ratio, which provided significant signal quality even though Mg Kα anode was used as the X-Ray source. Synchrotron light is expected to afford even higher quality and time resolution of XPS spectra.

N1s XPS signal for nitrogen gas can be directly compared to its QMS signal (amu 28) simultaneously recorded at the cell outlet. Shown in Figure 3(d), QMS signals generally reproduce the same pulse shape as N 1s signals, but with much higher signal-to-noise ratio. Closer inspection (see Figure 3(e)) of the rising pulse edge for height-normalized signals reveals that the QMS response is consistently delayed with respect to the XPS response by 3(±1) s. This delay can be attributed to the increased (doubled) distance in the gas lines between the injection point and the QMS as compared

to the injection point and the sample, which is in good agreement with the delay expected based on the vacuum conductance of the outlet line under these conditions (see Supplementary Note 3).

To further characterize the XPS and QMS signals, zeroth (m_0) and first (m_1) statistical moments were calculated for all transients after baseline correction (see Supplementary Note 2). Zeroth moments (i.e. area under the curve) are proportional to the amount of injected gas molecules (pulse size). Figure 3f demonstrates that the pulse size (normalized m_0) increases linearly with the increasing valve opening time (t_v) and that both QMS and XPS signals respond to this increase with comparable sensitivity. However, we note that the XPS-derived zeroth moment exhibits higher uncertainty due to its lower signal-to-noise ratio.

Both signals yield approximately the same mean residence time of gas molecules in the AP cell (τ_{res}) of 50(±2.5) s, which is independent of the valve opening time (Figure 3(g)). Comparison of the mean residence time and the average rising pulse edge delay of the QMS (50 s >> 3 s) suggests that the majority of molecules primarily reside within the AP cell, where they collide extensively with each other and with the cell walls before being evacuated either through the outlet or the nozzle of the electron analyzer. This is characteristic of a device with considerable degree of mixedness, despite the presence of relatively long inlet and outlet pipes.

Reproducibility of perturbations is another highly-desirable per-requisite for systematic transient kinetic experiments. In order to assess pulse reproducibility, a series of eighty pulses (t_v=4.5s) were supplied into the cell under otherwise constant conditions, and the variances of the corresponding responses were analyzed within the sequence. The response shapes were regressed (Levenberg-Marquardt algorithm) using a combination of a linear background and an exponential Gaussian pulse as a model (see Supplementary Note 2). The three independent parameters in this simple model (i.e. the pulse size, the mean delay, and the variance) were not strongly correlated to either each other or the pulse order within the sequence and were normally distributed around their mean values. Figure 3(h) illustrates a scatter plot of all 80 pulses, as relative deviations from the sample-mean, in three principal parametric dimensions: Area, FWHM, and Mean delay. The dataset

is scattered along the area and mean delay axes only within the 10% radius, although it is more broadly scattered along the FWHM axis (within 20%).

The amount of gas molecules injected per pulse can be estimated from the known flow rate of 1 sccm and pressure of 1 mbar that were observed at steady-state feed conditions prior to the pulsing experiment, i.e. with the pulsing valve fully open. Assuming the ideal gas law, the amount of molecules injected at valve opening time of 1s (t_v=1 s) can be estimated as

$$N_p = t_v \cdot \frac{Pv}{RT} = 1s \cdot \frac{100Pa \cdot (1.0/60) \cdot 10^{-6} m^3/s}{300K \cdot 8.314 J/mol/K} \approx 1 \cdot 10^{-9} mol \qquad (1).$$

We note that this estimate provides an upper bound of the pulse size, since in reality the pressure may not reach 1 mbar during the entire valve opening period due to a finite transient time. This "order of magnitude" estimate falls within the typical range of TAP experiments, which further illustrates that TAP and APXPS operate at similar pressure/temperature conditions and can potentially be combined in a fully reconciled transient spectro-kinetic experiment, albeit it is likely that despite considerable residence time in the cell not all gas molecules collide with the sample surface.

The overall reproducibility of pulses and the robustness of simple phenomenological pulse descriptors (Figures 3) achieved in this work constitute an important step towards the development of spectro-kinetic approaches involving APXPS. The inert gas-phase and surface tracer responses presented herein are already amenable to simple kinetic estimations within specified uncertainties. More systematic tracer studies would be necessary to fully understand the model of gas transport within the AP cell, highlighting the need for well-defined gas transport conditions that can be employed as standard processes for precise kinetic measurements, similarly to Knudsen diffusion in TAP. Nevertheless, the phenomenological values provided in this work for the mean (transport) residence time of gas inside the AP cell (including the gas lines) can readily be used to constrain the range of characteristic time scales for (chemical) kinetics that can be quantified under the used experimental conditions. Assuming an ideally-mixed reaction volume, i.e. Continuous Stirred-Tank Reactor (CSTR) in the AP cell, for which conversion is given[3] by

$$X = \frac{k_{app}\tau}{1+k_{app}\tau} \qquad (2),$$

a device with the mean residence time τ of 50 s can potentially provide kinetically-meaningful data (still subject to other, more stringent, criteria) with conversions between 0.05 and 0.95 for chemical processes with characteristic apparent rate constants k_{app} of 10^{-3}-10^{0} s^{-1}. The corresponding range of intrinsic rate constants k, $m^3 \cdot mol^{-1} \cdot s^{-1}$ can be estimated by taking into account a typical surface-to-volume ratio S_V in the AP cell (for a $5 \cdot 10^{-5}$ m^2 sample inside the $0.2 \cdot 10^{-3}$ m^3 AP cell) and a typical site-density a_S on a metal surface of $1 \cdot 10^{-6}$ $mol \cdot m^{-2}$:

$$k = \frac{k_{app}}{a_S S_V} \qquad (3),$$

resulting in the k range of ca. 10^3-10^6 $m^3 \cdot mol^{-1} \cdot s^{-1}$. In the context of heterogeneous catalysis, this range of values would correspond to extremely fast processes, comparable to the rates of oxygen dissociation on Pt at similar conditions[47]. These order-of-magnitude estimates indicate that kinetically-relevant transient APXPS experiments for a wide range of catalytic reactions with lower intrinsic rate constants can be implemented if the surface to volume ratio in the AP cell is considerably increased, for example, by employing samples comprised of porous films. For significantly slower reactions, the cell volume must also be reduced. For example, at 423K methanol reacts with oxygen atoms adsorbed on a surface of nanoporous gold with an intrinsic rate constant[48,49] of $k \sim 10^2$ $m^3 \cdot mol^{-1} \cdot s^{-1}$. Considering that the realistic oxygen coverage on this material is limited to fractions of a monolayer (0.01ML) due to the low oxygen dissociation probability, the apparent rate constant of this reaction would reach the lower bound of the sensitivity window if the volume of the cell is reduced to $2 \cdot 10^{-6}$ m^3, while the surface area is increased to $1 \cdot 10^{-4}$ m^2:

$$k_{app} = k a_S S_V = \frac{10^2 \cdot 0.01 \cdot 2.3 \cdot 10^{-5} \cdot 10^{-4}}{2 \cdot 10^{-6}} = 1 \cdot 10^{-3}\ s^{-1} \qquad (4),$$

where $2.3 \cdot 10^{-5}$ $mol \cdot m^{-2}$ is the atomic monolayer of a model Au(111) surface.

Aside from increasing the surface-to-volume ratio in the AP cell, experiments reported herein suggest potential avenues for further methodological improvements. Perturbations with even better control over the injected amounts, reproducibility, and gas transport times, comparable to those of TAP and modulation excitation techniques, could be achieved with deeper integration of hardware

components in future instruments, e.g. installing the gas injection valves in the immediate vicinity of the sample.

3.2. Pulse-wise titration of surface species

Monitoring the evolution of the sample surface within a series of many successive pulses is another useful mode of operation for the developed pulsing capabilities. This allows controlled preparation of specific surface states and systematic studies of surface changes (i.e. titration or well-defined state-altering TAP-like experiments[50]). To illustrate this operation mode, re-oxidation of a partially-reduced titanium oxide surface was used as an example (Figure 4). TiO_2 is a highly-relevant material in (photo)catalysis[51] and aerosol science[52,53], where its chemical properties are greatly affected by the surface oxidation state.

In this work, a single crystal of rutile TiO_2 exposing (110) surface (supplier: PI-KEM) was first reduced by Ar^+ ion sputtering (1.5 kV, 10 mA, $2 \cdot 10^{-5}$ mbar Ar, 20 min) which created oxygen vacancies. Then, the surface was gradually re-oxidized by injecting a train of O_2 pulses (1 s valve opening time, 60 s between pulses), while monitoring Ti 2p XPS spectra with DLD at an analyser pass energy of 50 eV, 3 mm slit width, and 100 ms dwell time for the image acquisition. The initial reduction and subsequent pulse-wise re-oxidation of the titania (110) surface are reflected prominently in its Ti 2p spectra, as shown in Figure 4a. Here, non-transient high-resolution Ti 2p XPS spectra are plotted for the initial (fully-oxidized, UHV reference), sputtered (deeply reduced), and partially re-oxidized (after 20 room temperature O_2 pulses) states of titania. Different oxidation states of Ti can clearly be distinguished in these spectra, in agreement with reference data on bulk materials[54] and recent APXPS measurements on Ti(110)[55]. The spectrum of the fully-oxidized TiO_2 (UHV reference) is composed of a characteristic Ti^{4+} doublet (due to spin-orbit coupling) with the more intense Ti^{4+} $2p^{3/4}$ component centered at 459.7 eV and a less intense Ti^{4+} $2p^{1/2}$ component centered at 465.5 eV, without any signs of Ti^{3+}. The spectrum of sputtered titania features an additional spin-orbit pair of Ti^{3+} 2p components which are shifted with respect to Ti^{4+} to lower binding energies.

In the partially re-oxidized spectrum, the intensity ratio between the two predominant oxidation states Ti^{4+}/Ti^{3+} is shifted back towards the fully-oxidized UHV reference. Even without rigorous deconvolution of these complex spectra, which was not pursued in these proof of principle studies, it can be seen that the ratio between the integrated intensities within the Ti^{4+} and Ti^{3+} bands (Ti^{4+}/Ti^{3+}) can be used as a descriptor of the average surface oxidation state.

To quantify the average surface oxidation state during the re-oxidation pulse sequence, the acquired raw DLD spectra were binned in time and integrated in two spectral regions representative of the Ti^{4+} species (channels 320-440 or 460.14-459.13 eV) and Ti^{3+} species (channels 470-650 or 458.88-457.38 eV) . These spectral ranges are highlighted in Figure 4(c) for DLD snapshots and in Figure 4(a) for reference spectra. The initial state of the sputtered, partially reduced TiO_2 was characterized by the ratio of Ti^{4+}/Ti^{3+} spectral regions of 0.9 in the raw DLD data, which agreed well with the corresponding ratio of 0.86 in the full scan Figure 4(a). The evolution of the Ti^{4+}/Ti^{3+} ratio during an ensuing series of oxygen pulses demonstrated the ability to precisely control the oxidation state of the titania surface within the 0.9-1.2 range of the Ti^{4+}/Ti^{3+} ratio. The resulting nominal Ti^{4+}/Ti^{3+} ratio increased with the number of injected oxygen pulses, as expected from the re-oxidation process (see Figure 4(d)). Furthermore, several regimes in the re-oxidation kinetics could be clearly distinguished: the initial rapid increase in the Ti^{4+}/Ti^{3+} ratio during the first five pulses at room temperature, followed by a slower (linear) increase with the slope largely unaffected by the temperature change from room temperature to 100 ºC. A similar pattern was observed again, while the material was further re-oxidized at a higher temperature of 200 ºC. Comparison with the fully oxidized UHV reference in Figure 4(a), which exhibited a nominal Ti^{4+}/Ti^{3+} descriptor ratio of 2 despite not containing Ti^{+3} (integration artifact), reveals that the surface was not completely oxidized into the original stoichiometric TiO_2 by the end of the pulse sequence at 200 ºC. It should be noted, however, that this comparison is also affected by the difference in backgrounds in the two data acquisition modes.

Drawing parallels with multi-pulse TAP experiments, the sequence-based experimental approach in APXPS presents novel opportunities for systematic characterization of chemically-reactive and dynamically evolving surfaces. For example, the rate of O-vacancy diffusion from the bulk of the material can be evaluated by monitoring the chemical state of the surface with XPS after a pre-defined number of pulses has been delivered. Likewise, pulse sequences of reagent molecules can be used to prepare and probe chemical properties of well-defined surface states in catalysis e.g. see Shekhtman et al.[50]or Wang and Makkee[56]. We note that in the specific example of multi-pulse data presented in Figure 4, the evolution of titania surface occurred on relatively slow time scale, which could have been captured by less time-resolved data acquisition mode. However, in the future, the newly developed synchronization capabilities will facilitate quantitative reconciliation of the kinetic and spectroscopic data related to a broader range of reaction kinetics.

3.3. Precursor delivery for Atomic Layer Deposition (ALD)

A pulsed valve system similar to the one described in this paper is commonly employed in Atomic Layer Deposition (ALD) processes[57]. In ALD, a substrate is exposed periodically and alternatingly to different precursor gases which create - under ideal conditions - atomically thin, conformal layers of materials, depending on the precursors used. Thicknesses of these films can be controlled accurately and simply by the number of deposition cycles repeated. APXPS measurements have emerged as a valuable source of fundamental information about the surface reactions involved in ALD[58–61]. We have used the pulsed valve system together with the RPi electronics to automate the pulsing of the precursor gases in order to study ALD processes *in-situ* using APXPS.

For the ALD experiments, the gas lines and the pulsed valves were slightly re-configured from the experiments described above, as shown in Figure 5. In this case, there had to be two inlet tubes to the AP cell, one for each precursor, and at least one pulsed valve in each inlet tube in order to supply reagents for the both ALD half-cycles. Likewise, the Python script controlling the valves was adjusted to implement the sequential injection of ALD precursors. As the programming is done fully in the

Python environment, it is easily adaptable to different applications and relatively quick to reprogram in order to meet different experimental needs and more complicated pulsing sequences. In this case, the program emulated pulse-purge-pulse-purge cycles of an ALD process, in which titania (TiO_2) layers were grown on a silicon substrate at 200 ºC.

The pulsing sequence (see Figure 6(a)) consisted of an exposure to titanium (IV) tetraisopropoxide (TTIP) – the source of titanium – followed by a period of purging with inert gas the cell, and then followed by an exposure to water – the source of oxygen. A final purge period completed the cycle, after which another ALD cycle could begin. Figure 6(b) demonstrates an example of APXPS data recorded during the first (TTIP) half-cycle (t_v = 2000s). The XPS was measured in a snapshot mode, with a fixed kinetic energy window focusing on the Ti 2p region at a binding energy of approximately 460 eV. A considerable delay between the pulse injection and the appearance of the surface Ti signal in XPS is caused by the reaction of the TTIP precursor with surfaces of the feed lines and the APXPS cell that have either never been exposed to the precursor before or have been exposed to water prior to the TTIP injection. The TiO_2 growth on the sample surface is observed only after all preceding surfaces are saturated with the precursor.

Overall, this example clearly demonstrates the utility of programmable perturbations of gas composition fully synchronized with the APXPS data acquisition for reproducibility of ALD cycles in the APXPS spectroscopic cell and, potentially, for acquiring time-resolved APXPS data on the kinetics of ALD growth reactions. One must note, though, that the time constants of the cell are still too large to capture kinetics of the most relevant ALD processes that are completed in fractions of seconds in actual ALD reactors. In other words, the current setup appears to operate in a transport-limited rather than reaction-limited mode. Therefore, the main value of these experiments is expected to lie in chemical identification of the surface intermediates formed in each ALD reaction step.

4. Conclusion and perspectives

A hardware/software interface is described that allows for the injection of well-defined gas pulses into an APXPS cell on the same time frame, i.e. fully synchronized, with the triggering of a DLD XPS detector. This interface enables a number of fast, time-resolved, perturbation-enhanced APXPS experiments to be systematically performed with a wide variety of materials and reactions. The synchronizing interface was implemented at the APXPS branch of the SPECIES beamline at MAX IV Laboratory, based on a Rasberry Pi controller with Python API and a number of other easily accessible components. The capabilities of this approach were illustrated by three experimental examples. First, N_2 pulsing over Au foil demonstrated that XPS signals, in this case N 1s and Au 4f, can be monitored with sub-second time resolution for a single gas pulse. In combination with downstream QMS data, these pulses demonstrated that the APXPS cell has a characteristic residence time of 50s, which can tentatively be assigned to the inner well-mixed volume of the cell, rather than the upstream and downstream feed lines. Second, Ti 2p XPS spectra recorded during a multi-pulse sequence of O_2 injections over pre-reduced TiO_2 were used to quantitatively monitor the evolution of Ti oxidation state, which revealed a non-trivial behavior of re-oxidation kinetics. Finally, time-resolved XPS data were presented for the precursor-loading half-cycle of an ALD process for TiO_2 deposition.

Although developed for model systems already in the early days of surface science, such experiments with synchronous gas perturbations and surface characterization have not found their way into the standard repertoire of modern APXPS measurements, partially because the methodology development efforts were primarily focused on maximizing the pressure of reactants in the vicinity of the sample. Perturbation-enhanced APXPS experiments developed herein were inspired by the success of pulse-response TAP experiments in elucidating the intrinsic kinetics of gas-solid reactions on complex materials from gaseous perspective. We foresee that perturbation-enhanced APXPS approach will provide complementary time-resolve data from surface perspective, which eventually

can be reconciled with gaseous reaction kinetics for a more in depth understanding of underlying structure-activity relationships in catalysis and beyond.

Supplementary Material

See Supplementary Material for the detailed descriptions of (1) the synchronization circuitry and (2) data treatment that was employed in the analysis of gas pulses.

Acknowledgments

This work was supported by the funding provided by the Research Council of Norway (RCN) under the contract #272266 (TAPXPS project) and the European Regional Development Fund (Interreg Öresun-Kattegat-Skagerrak ESS & MAX IV: Cross Border Science and Society, MAX4ESSFUN, Ref. no. MAX-004). SU acknowledges funding from the European Research Council under the European Union's Horizon2020 research and innovation program, project SURFACE (grant agreement no. 717022) and the Academy of Finland (grant no. 326291). The ALD-related research was financed by the Faculty of Science, University of Helsinki and Academy of Finland (grants 295696 and 309552). We acknowledge MAX IV Laboratory for time on the SPECIES beamline. Research conducted at MAX IV, a Swedish national user facility, is supported by the Swedish Research council under contract 2018-07152, the Swedish Governmental Agency for Innovation Systems under contract 2018-04969, and Formas under contract 2019-02496. The authors acknowledge technical support by many colleagues at MAX-IV and UiO. Last, but not least, the authors would like to express their gratitude for many inspiring discussions with Prof. John Gleaves and Mr. John Gleaves Jr. of Mithra Technologies (USA), Dr. Rebecca Fushimi of Idaho National Laboratory (USA), Prof. Joachim Schnadt of Lund University (Sweden), and Dr. Spyros Diplas of SINTEF Industry (Norway), which contributed to finding many solutions, asking even more questions, and maintaining the spirit of adventure during this work.

Data Availability Statement

The data that support the findings of this study are available from the corresponding author upon reasonable request.

Figure captions

Figure 1. A general scheme of the APXPS cell with a sample, the gas feeding section, and the electron analyzer. The insets show the imposed (square pulse) gas perturbation on the same time scale with the QMS signal at the cell outlet (left) and the synchronized DLD XPS signal recorded from the sample surface (right).

Figure 2. The operating principles of pneumatic valves which actuation was synchronized with the DLD detector via RPi: (a) gas injection mode and (b) gas bypass mode.

Figure 3. A transient (pulse-response) APXPS experiment (Mg Kα X-Ray source) enabled by the synchronization interface: (a) temporal profile of the gas perturbation (pulse); (b) N 1s and (c) Au 4f transients recorded by DLD after single N2 pulses over gold foil, comparing responses for different valve-opening times (tv); (d) QMS signal at amu 28 recorded at the cell outlet for different tv; (e) the time difference between the raising N 1S XPS vs. QMS signals; (f) normalized zeroth moments and (g) mean residence times of N 1s XPS (DLD) and QMS signals as functions of valve-opening times tv; (h) reproducibility of pulse characteristics (relative deviations from the sample-mean values of the center, size, and width), the ovoid depicts the maximal encompassing volume for the entire dataset.

Figure 4. A multi-pulse APXPS experiments (Mg Kα X-Ray source) with re-oxidation of pre-reduced TiO2 (110) single crystal. (a) High-resolution scans of the initial fully-oxidized surface in UHV (bottom), partially reduced, sputtered surface (middle), and partially re-oxidized surface after O2

pulses; (b) a schematic representation of the pulsing sequence used for the crystal re-oxidation; (c) examples of raw DLD spectra after the first and 20th pulses; (d) The nominal Ti4+/Ti3+ ratio as a function of O2 exposure at various temperatures. Data binned to 34 s (grey line) and 1 individual pulse (blue squares) to illustrate the trade–off between the temporal resolution and signal–to–noise ratio. The Ti4+/Ti3+ ratio was obtained by integrating the corresponding spectral regions that are highlighted in grey in panels (a) and (c).

Figure 5. The operation of pneumatic valves during ALD half-cycles: (a) metal precursor injection and (b) water injection.

Figure 6. Use of synchronized valves for ALD: (a) the pulsing sequence used for TiO_2 deposition and (b) time-resolved APXPS data during the TTIP precursor pulse recorded using the Mg Kα X-ray source.

References

(1) Bennett, C. O. Understanding Heterogeneous Catalysis Through the Transient Method. In *Catalysis Under Transient Conditions*; Bell, A. T., Hegedus, L. L., Eds.; AMERICAN CHEMICAL SOCIETY: WASHINGTON, D. C., 1982; Vol. 178, pp 1–32. https://doi.org/10.1021/bk-1982-0178.ch001.

(2) Tamaru, K. Dynamic Relaxation Methods in Heterogeneous Catalysis. In *Catalysis: Science and Technology*; Anderson, J. R., Boudart, M., Eds.; Catalysis; Springer: Berlin, Heidelberg, 1991; pp 87–129. https://doi.org/10.1007/978-3-642-75956-7_2.

(3) Marin, G. B.; Yablonsky, G. S. *Kinetics of Chemical Reactions: Decoding Complexity*; Wiley-VCH, 2011.

(4) Happel, J. Transient Tracing. *Chemical Engineering Science* **1978**, *33* (11), 1567. https://doi.org/10.1016/0009-2509(78)85214-2.

(5) Shannon, S. L.; Goodwin, J. G. Characterization of Catalytic Surfaces by Isotopic-Transient Kinetics during Steady-State Reaction. *Chem. Rev.* **1995**, *95* (3), 677–695. https://doi.org/10.1021/cr00035a011.

(6) Ledesma, C.; Yang, J.; Chen, D.; Holmen, A. Recent Approaches in Mechanistic and Kinetic Studies of Catalytic Reactions Using SSITKA Technique. *ACS Catal.* **2014**, 4527–4547. https://doi.org/10.1021/cs501264f.

(7) Bundhoo, A.; Schweicher, J.; Frennet, A.; Kruse, N. Chemical Transient Kinetics Applied to CO Hydrogenation over a Pure Nickel Catalyst. *J. Phys. Chem. C* **2009**, *113* (24), 10731–10739. https://doi.org/10.1021/jp902647z.

(8) Yasuda, Y.; Mizusawa, H.; Kamimura, T. Frequency Response Method for Investigation of Kinetic Details of a Heterogeneous Catalyzed Reaction of Gases. *J. Phys. Chem. B* **2002**, *106* (26), 6706–6712. https://doi.org/10.1021/jp014295u.

(9) Zhdanov, V. P. Periodic Perturbation of the Kinetics of Heterogeneous Catalytic Reactions. *Surface Science Reports* **2004**, *55* (1), 1–48. https://doi.org/10.1016/j.surfrep.2004.06.001.

(10) Scalbert, J.; Meunier, F. C.; Daniel, C.; Schuurman, Y. An Operando DRIFTS Investigation into the Resistance against CO_2 Poisoning of a Rh/Alumina Catalyst during Toluenehydrogenation. *Phys. Chem. Chem. Phys.* **2012**, *14* (7), 2159–2163. https://doi.org/10.1039/C1CP22620G.

(11) Newton, M. A. Time Resolved Operando X-Ray Techniques in Catalysis, a Case Study: CO Oxidation by O2 over Pt Surfaces and Alumina Supported Pt Catalysts. *Catalysts* **2017**, *7* (2), 58. https://doi.org/10.3390/catal7020058.

(12) Minova, I. B.; Matam, S. K.; Greenaway, A.; Catlow, C. R. A.; Frogley, M. D.; Cinque, G.; Wright, P. A.; Howe, R. F. Elementary Steps in the Formation of Hydrocarbons from Surface Methoxy Groups in HZSM-5 Seen by Synchrotron Infrared Microspectroscopy. *ACS Catal.* **2019**, *9* (7), 6564–6570. https://doi.org/10.1021/acscatal.9b01820.

(13) Urakawa, A.; Bürgi, T.; Baiker, A. Sensitivity Enhancement and Dynamic Behavior Analysis by Modulation Excitation Spectroscopy: Principle and Application in Heterogeneous Catalysis. *Chemical Engineering Science* **2008**, *63* (20), 4902–4909. https://doi.org/10.1016/j.ces.2007.06.009.

(14) Ferri, D.; Newton, M. A.; Nachtegaal, M. Modulation Excitation X-Ray Absorption Spectroscopy to Probe Surface Species on Heterogeneous Catalysts. *Top Catal* **2011**, *54* (16–18), 1070–1078. https://doi.org/10.1007/s11244-011-9727-5.

(15) Baurecht, D.; Fringeli, U. P. Quantitative Modulated Excitation Fourier Transform Infrared Spectroscopy. *Review of Scientific Instruments* **2001**, *72* (10), 3782–3792. https://doi.org/doi:10.1063/1.1400152.

(16) Gleaves, J. T.; Ebner, J. R.; Kuechler, T. C. Temporal Analysis of Products (TAP) - A Unique Catalyst Evaluation System with Submillisecond Time Resolution. *Catalysis Reviews* **1988**, *30* (1), 49–116. https://doi.org/10.1080/01614948808078616.

(17) Gleaves, J. T.; Yablonsky, G.; Zheng, X.; Fushimi, R.; Mills, P. L. Temporal Analysis of Products (TAP) - Recent Advances in Technology for Kinetic Analysis of Multi-Component Catalysts. *Journal of Molecular Catalysis A: Chemical* **2010**, *315* (2), 108–134. https://doi.org/10.1016/j.molcata.2009.06.017.

(18) Yablonsky, G. S.; Olea, M.; Marin, G. B. Temporal Analysis of Products: Basic Principles, Applications, and Theory. *Journal of Catalysis* **2003**, *216* (1–2), 120–134. https://doi.org/10.1016/S0021-9517(02)00109-4.

(19) Morgan, K.; Maguire, N.; Fushimi, R.; Gleaves, J. T.; Goguet, A.; Harold, M. P.; Kondratenko, E. V.; Menon, U.; Schuurman, Y.; Yablonsky, G. S. Forty Years of Temporal Analysis of Products. *Catal. Sci. Technol.* **2017**, *7* (12), 2416–2439. https://doi.org/10.1039/C7CY00678K.

(20) Widmann, D.; Behm, R. J. Activation of Molecular Oxygen and the Nature of the Active Oxygen Species for CO Oxidation on Oxide Supported Au Catalysts. *Acc. Chem. Res.* **2014**, *47* (3), 740–749. https://doi.org/10.1021/ar400203e.

(21) Yablonsky, G. S.; Redekop, E. A.; Constales, D.; Gleaves, J. T.; Marin, G. B. Rate-Reactivity Model: A New Theoretical Basis for Systematic Kinetic Characterization of Heterogeneous Catalysts. *International Journal of Chemical Kinetics* **2016**, *48* (6), 304–317. https://doi.org/10.1002/kin.20988.

(22) Roy, K.; Artiglia, L.; Bokhoven, J. A. van. Ambient Pressure Photoelectron Spectroscopy: Opportunities in Catalysis from Solids to Liquids and Introducing Time Resolution. *ChemCatChem* **2018**, *10* (4), 666–682. https://doi.org/10.1002/cctc.201701522.

(23) Rubloff, G. W. Photoemission Studies of Time-Resolved Surface Reactions: Isothermal Desorption of CO from Ni(111). *Surface Science* **1979**, *89* (1), 566–574. https://doi.org/10.1016/0039-6028(79)90638-1.

(24) Steinbach, F.; Schütte, J. Time-resolved Photoelectron Spectroscopy for the Study of Dynamic Surface Species. *Review of Scientific Instruments* **1983**, *54* (9), 1169–1174. https://doi.org/10.1063/1.1137544.

(25) D'Evelyn, M. P.; Madix, R. J. Reactive Scattering from Solid Surfaces. *Surface Science Reports* **1983**, *3* (8), 413–495. https://doi.org/10.1016/0167-5729(83)90002-X.

(26) Libuda, J. Molecular Beams and Model Catalysis: Activity and Selectivity of Specific Reaction Centers on Supported Nanoparticles. *Chemphyschem* **2004**, *5* (5), 625–631. https://doi.org/10.1002/cphc.200400049.

(27) Zaera, F. Use of Molecular Beams for Kinetic Measurements of Chemical Reactions on Solid Surfaces. *Surface Science Reports* **2017**, *72* (2), 59–104. https://doi.org/10.1016/j.surfrep.2017.02.002.

(28) Amati, M.; Abyaneh, M. K.; Gregoratti, L. Dynamic High Pressure: A Novel Approach toward near Ambient Pressure Photoemission Spectroscopy and Spectromicroscopy. *J. Inst.* **2013**, *8* (05), T05001–T05001. https://doi.org/10.1088/1748-0221/8/05/T05001.

(29) Schnadt, J.; Knudsen, J.; Johansson, N. Present and New Frontiers in Materials Research by Ambient Pressure X-Ray Photoelectron Spectroscopy. *J. Phys.: Condens. Matter* **2020**. https://doi.org/10.1088/1361-648X/ab9565.

(30) Salmeron, M.; Schlogl, R. Ambient Pressure Photoelectron Spectroscopy: A New Tool for Surface Science and Nanotechnology. *Surface Science Reports* **2008**, *63* (4), 169–199. https://doi.org/10.1016/j.surfrep.2008.01.001.

(31) Trotochaud, L.; Head, A. R.; Karslıoğlu, O.; Kyhl, L.; Bluhm, H. Ambient Pressure Photoelectron Spectroscopy: Practical Considerations and Experimental Frontiers. *J. Phys.: Condens. Matter* **2016**, *29* (5), 053002. https://doi.org/10.1088/1361-648X/29/5/053002.

(32) Nguyen, L.; Tao, F. F.; Tang, Y.; Dou, J.; Bao, X.-J. Understanding Catalyst Surfaces during Catalysis through Near Ambient Pressure X-Ray Photoelectron Spectroscopy. *Chem. Rev.* **2019**, *119* (12), 6822–6905. https://doi.org/10.1021/acs.chemrev.8b00114.

(33) Arble, C.; Jia, M.; Newberg, J. T. Lab-Based Ambient Pressure X-Ray Photoelectron Spectroscopy from Past to Present. *Surface Science Reports* **2018**, *73* (2), 37–57. https://doi.org/10.1016/j.surfrep.2018.02.002.

(34) Knudsen, J.; Andersen, J. N.; Schnadt, J. A Versatile Instrument for Ambient Pressure X-Ray Photoelectron Spectroscopy: The Lund Cell Approach. *Surface Science* **2016**, *646*, 160–169. https://doi.org/10.1016/j.susc.2015.10.038.

(35) Schnadt, J.; Knudsen, J.; Andersen, J. N.; Siegbahn, H.; Pietzsch, A.; Hennies, F.; Johansson, N.; Mårtensson, N.; Öhrwall, G.; Bahr, S.; Mähl, S.; Schaff, O. The New Ambient-Pressure X-Ray Photoelectron Spectroscopy Instrument at MAX-Lab. *J Synchrotron Rad* **2012**, *19* (5), 701–704. https://doi.org/10.1107/S0909049512032700.

(36) Amann, P.; Degerman, D.; Lee, M.-T.; Alexander, J. D.; Shipilin, M.; Wang, H.-Y.; Cavalca, F.; Weston, M.; Gladh, J.; Blom, M.; Björkhage, M.; Löfgren, P.; Schlueter, C.; Loemker, P.; Ederer, K.; Drube, W.; Noei, H.; Zehetner, J.; Wentzel, H.; Åhlund, J.; Nilsson, A. A High-Pressure x-Ray Photoelectron Spectroscopy Instrument for Studies of Industrially Relevant Catalytic Reactions at Pressures of Several Bars. *Review of Scientific Instruments* **2019**, *90* (10), 103102. https://doi.org/10.1063/1.5109321.

(37) Salmeron, M. From Surfaces to Interfaces: Ambient Pressure XPS and Beyond. *Top Catal* **2018**, *61* (20), 2044–2051. https://doi.org/10.1007/s11244-018-1069-0.

(38) Velasco-Vélez, J. J.; Pfeifer, V.; Hävecker, M.; Wang, R.; Centeno, A.; Zurutuza, A.; Algara-Siller, G.; Stotz, E.; Skorupska, K.; Teschner, D.; Kube, P.; Braeuninger-Weimer, P.; Hofmann, S.; Schlögl, R.; Knop-Gericke, A. Atmospheric Pressure X-Ray Photoelectron Spectroscopy Apparatus: Bridging the Pressure Gap. *Review of Scientific Instruments* **2016**, *87* (5), 053121. https://doi.org/10.1063/1.4951724.

(39) Keller, H.; Klingelhöfer, G.; Kankeleit, E. A Position Sensitive Microchannelplate Detector Using a Delay Line Readout Anode. *Nuclear Instruments and Methods in Physics Research Section A: Accelerators, Spectrometers, Detectors and Associated Equipment* **1987**, *258* (2), 221–224. https://doi.org/10.1016/0168-9002(87)90059-3.

(40) Lampton, M.; Siegmund, O.; Raffanti, R. Delay Line Anodes for Microchannel-plate Spectrometers. *Review of Scientific Instruments* **1987**, *58* (12), 2298–2305. https://doi.org/10.1063/1.1139341.

(41) Weststrate, C. J. (Kees-J.; Sharma, D.; Garcia Rodriguez, D.; Gleeson, M. A.; Fredriksson, H. O. A.; Niemantsverdriet, J. W. (Hans). Mechanistic Insight into Carbon-Carbon Bond Formation on Cobalt under Simulated Fischer-Tropsch Synthesis Conditions. *Nature Communications* **2020**, *11* (1), 750. https://doi.org/10.1038/s41467-020-14613-5.

(42) Artiglia, L.; Orlando, F.; Roy, K.; Kopelent, R.; Safonova, O.; Nachtegaal, M.; Huthwelker, T.; van Bokhoven, J. A. Introducing Time Resolution to Detect Ce3+ Catalytically Active Sites at the Pt/CeO2 Interface through Ambient Pressure X-Ray Photoelectron Spectroscopy. *J. Phys. Chem. Lett.* **2017**, *8* (1), 102–108. https://doi.org/10.1021/acs.jpclett.6b02314.

(43) Urpelainen, S.; Såthe, C.; Grizolli, W.; Agåker, M.; Head, A. R.; Andersson, M.; Huang, S.-W.; Jensen, B. N.; Wallén, E.; Tarawneh, H.; Sankari, R.; Nyholm, R.; Lindberg, M.; Sjöblom, P.; Johansson, N.; Reinecke, B. N.; Arman, M. A.; Merte, L. R.; Knudsen, J.; Schnadt, J.; Andersen, J. N.; Hennies, F. The SPECIES Beamline at the MAX IV Laboratory: A Facility for Soft X-Ray RIXS and APXPS. *J Synchrotron Rad* **2017**, *24* (1), 344–353. https://doi.org/10.1107/S1600577516019056.

(44) Kokkonen, E.; Lopes da Silva, F.; Mikkela, M.-H.; Johansson, N.; Huang, S.-W.; Lee, J.-M.; Andersson, M.; Bartalesi, A.; Reinecke, B.; Handrup, K.; Tarawneh, H.; Sankari, R.; Knudsen, J.; Schnadt, J.; Sathe, C.; Urpelainen, S. Upgrade of the SPECIES Beamline at the MAX IV Laboratory. *Journal of Synchrotron Radiation* **2021**, *28*. https://doi.org/10.1107/S1600577521000564.

(45) Halfacree, G.; Upton, E. *Raspberry Pi User Guide*, 1st ed.; Wiley Publishing, 2012.

(46) Fitzpatrick, D. E.; O'Brien, M.; Ley, S. V. A Tutored Discourse on Microcontrollers, Single Board Computers and Their Applications to Monitor and Control Chemical Reactions. *React. Chem. Eng.* **2020**, *5* (2), 201–220. https://doi.org/10.1039/C9RE00407F.

(47) Redekop, E. A.; Yablonsky, G. S.; Constales, D.; Ramachandran, P. A.; Pherigo, C.; Gleaves, J. T. The Y-Procedure Methodology for the Interpretation of Transient Kinetic Data: Analysis of Irreversible Adsorption. *Chemical Engineering Science* **2011**, *66* (24), 6441–6452. https://doi.org/10.1016/j.ces.2011.08.055.

(48) Wang, L.-C.; Friend, C. M.; Fushimi, R.; Madix, R. J. Active Site Densities, Oxygen Activation and Adsorbed Reactive Oxygen in Alcohol Activation on NpAu Catalysts. *Faraday Discuss.* **2016**, *188* (0), 57–67. https://doi.org/10.1039/C5FD00161G.

(49) Reece, C.; Redekop, E. A.; Karakalos, S.; Friend, C. M.; Madix, R. J. Crossing the Great Divide between Single-Crystal Reactivity and Actual Catalyst Selectivity with Pressure Transients. *Nature Catalysis* **2018**, *1* (11), 852–859. https://doi.org/10.1038/s41929-018-0167-5.

(50) Shekhtman, S. O.; Yablonsky, G. S.; Gleaves, J. T.; Fushimi, R. "State Defining" Experiment in Chemical Kinetics - Primary Characterization of Catalyst Activity in a TAP Experiment. *Chemical Engineering Science* **2003**, *58* (21), 4843–4859. https://doi.org/10.1016/j.ces.2003.08.005.

(51) Schneider, J.; Matsuoka, M.; Takeuchi, M.; Zhang, J.; Horiuchi, Y.; Anpo, M.; Bahnemann, D. W. Understanding TiO2 Photocatalysis: Mechanisms and Materials. *Chem. Rev.* **2014**, *114* (19), 9919–9986. https://doi.org/10.1021/cr5001892.

(52) Nicolas, M.; Ndour, M.; Ka, O.; D'Anna, B.; George, C. Photochemistry of Atmospheric Dust: Ozone Decomposition on Illuminated Titanium Dioxide. *Environ. Sci. Technol.* **2009**, *43* (19), 7437–7442. https://doi.org/10.1021/es901569d.

(53) Chen, Y.; Tong, S.; Wang, J.; Peng, C.; Ge, M.; Xie, X.; Sun, J. Effect of Titanium Dioxide on Secondary Organic Aerosol Formation. *Environ. Sci. Technol.* **2018**, *52* (20), 11612–11620. https://doi.org/10.1021/acs.est.8b02466.

(54) Kurtz, R. L.; Henrich, V. E. Comparison of Ti 2p Core-Level Peaks from TiO2, Ti2O3, and Ti Metal, by XPS. *Surface Science Spectra* **1998**, *5* (3), 179–181. https://doi.org/10.1116/1.1247874.

(55) Jackman, M. J.; Thomas, A. G.; Muryn, C. Photoelectron Spectroscopy Study of Stoichiometric and Reduced Anatase TiO2(101) Surfaces: The Effect of Subsurface Defects on Water Adsorption at Near-Ambient Pressures. *J. Phys. Chem. C* **2015**, *119* (24), 13682–13690. https://doi.org/10.1021/acs.jpcc.5b02732.

(56) Wang, Y.; Makkee, M. Fundamental Understanding of the Di-Air System (an Alternative NOx Abatement Technology). I: The Difference in Reductant Pre-Treatment of Ceria. *Applied Catalysis B: Environmental* **2018**, *223*, 125–133. https://doi.org/10.1016/j.apcatb.2017.04.054.

(57) Suntola, T.; Hyvarinen, J. Atomic Layer Epitaxy. *Annu. Rev. Mater. Sci.* **1985**, *15* (1), 177–195. https://doi.org/10.1146/annurev.ms.15.080185.001141.

(58) Head, A. R.; Chaudhary, S.; Olivieri, G.; Bournel, F.; Andersen, J. N.; Rochet, F.; Gallet, J.-J.; Schnadt, J. Near Ambient Pressure X-Ray Photoelectron Spectroscopy Study of the Atomic Layer Deposition of TiO2 on RuO2(110). *J. Phys. Chem. C* **2016**, *120* (1), 243–251. https://doi.org/10.1021/acs.jpcc.5b08699.

(59) Timm, R.; Head, A. R.; Yngman, S.; Knutsson, J. V.; Hjort, M.; McKibbin, S. R.; Troian, A.; Persson, O.; Urpelainen, S.; Knudsen, J.; Schnadt, J.; Mikkelsen, A. Self-Cleaning and Surface Chemical Reactions during Hafnium Dioxide Atomic Layer Deposition on Indium Arsenide. *Nature Communications* **2018**, *9* (1), 1412. https://doi.org/10.1038/s41467-018-03855-z.

(60) Temperton, R. H.; Gibson, A.; O'Shea, J. N. In Situ XPS Analysis of the Atomic Layer Deposition of Aluminium Oxide on Titanium Dioxide. *Phys. Chem. Chem. Phys.* **2019**, *21* (3), 1393–1398. https://doi.org/10.1039/C8CP06912C.

(61) D'Acunto, G.; Troian, A.; Kokkonen, E.; Rehman, F.; Liu, Y.-P.; Yngman, S.; Yong, Z.; McKibbin, S. R.; Gallo, T.; Lind, E.; Schnadt, J.; Timm, R. Atomic Layer Deposition of Hafnium Oxide on InAs: Insight from Time-Resolved in Situ Studies. *ACS Appl. Electron. Mater.* **2020**. https://doi.org/10.1021/acsaelm.0c00775.

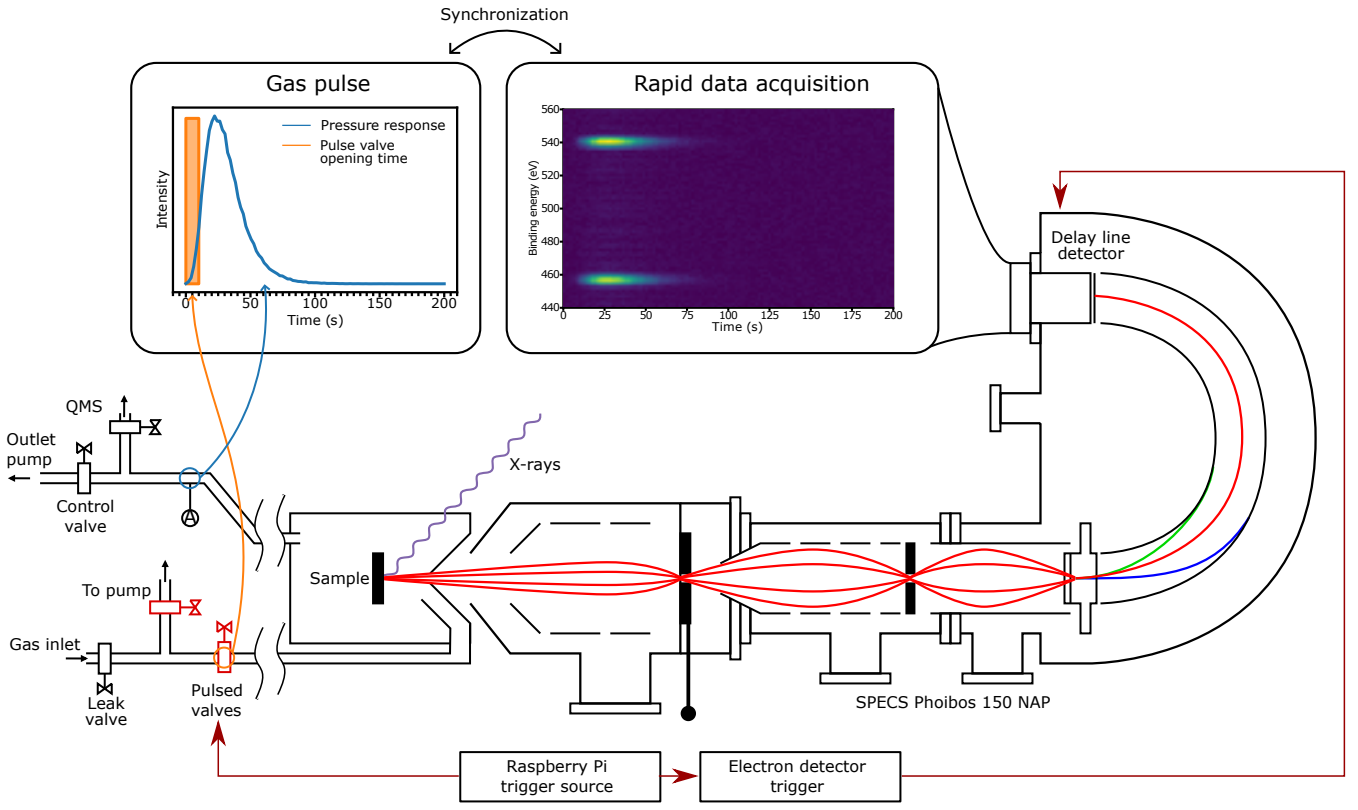
Synchronization
Gas pulse
Pressure response
Pulse valve opening time
Intensity
Time (s)
Rapid data acquisition
Binding energy (eV)
Time (s)
Delay line detector
QMS
Outlet pump
Control valve
X-rays
Sample
To pump
Gas inlet
Leak valve
Pulsed valves
SPECS Phoibos 150 NAP
Raspberry Pi trigger source
Electron detector trigger

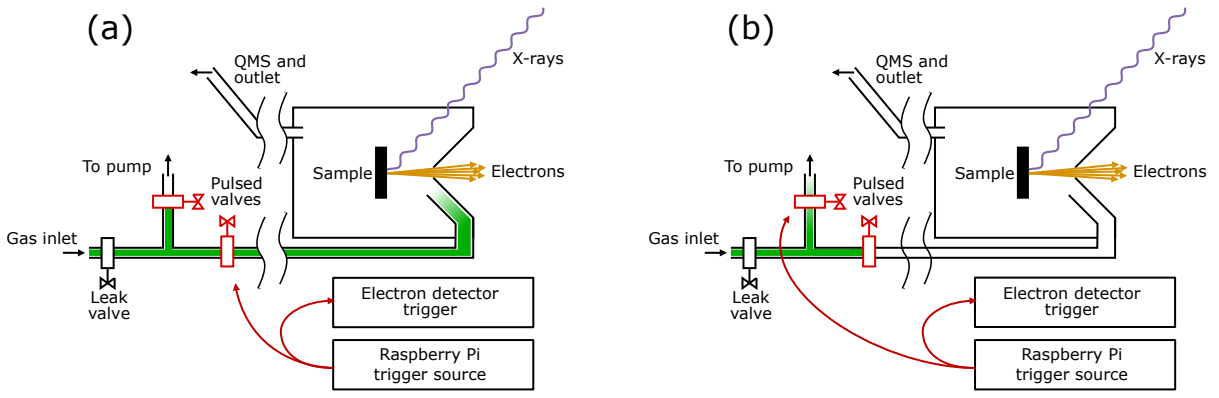
(a)
QMS and outlet
X-rays
To pump
Pulsed valves
Sample
Electrons
Gas inlet
Leak valve
Electron detector trigger
Raspberry Pi trigger source
(b)
QMS and outlet
X-rays
To pump
Pulsed valves
Sample
Electrons
Gas inlet
Leak valve
Electron detector trigger
Raspberry Pi trigger source

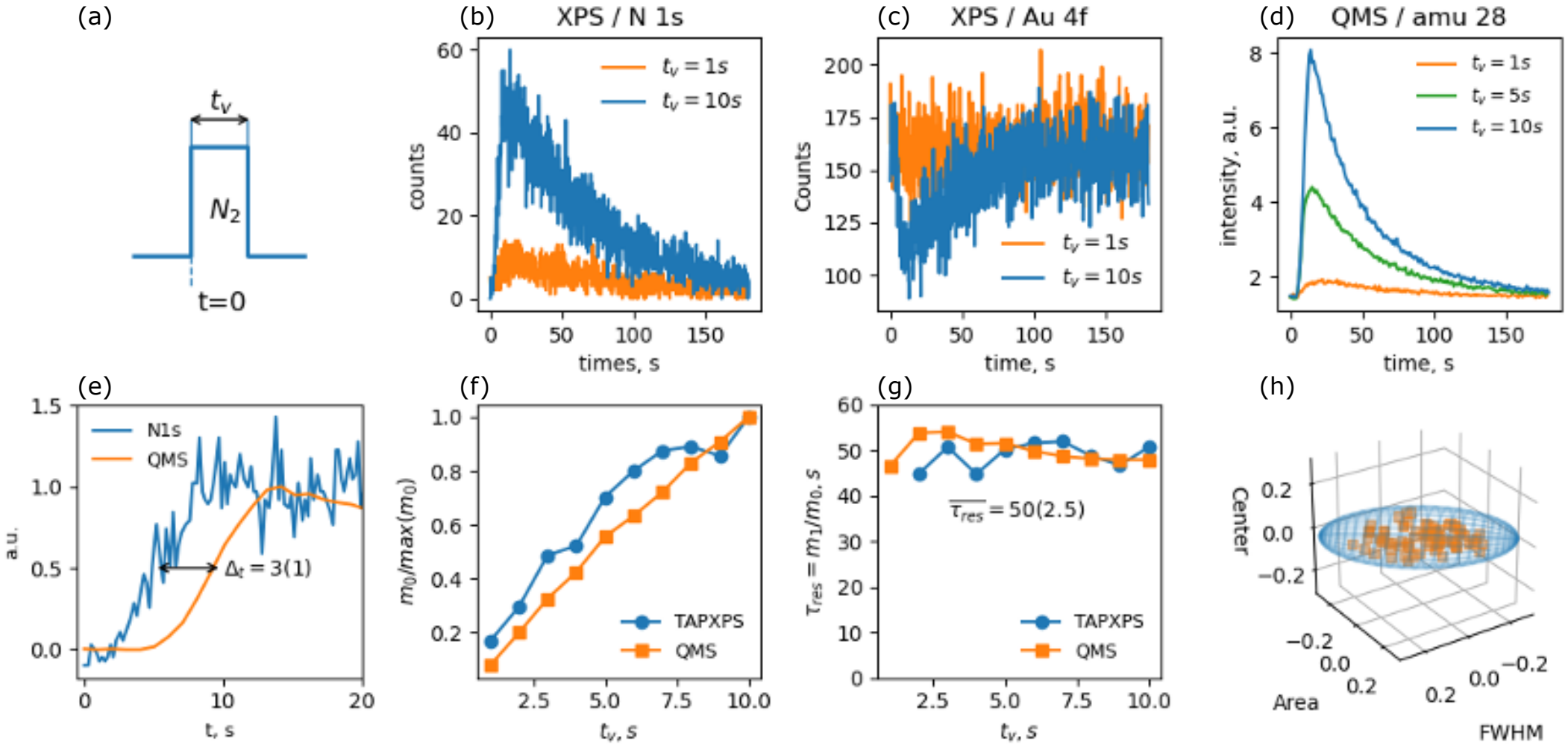
(a)
t_v
N_2
t=0
(b)
XPS / N 1s
$t_v = 1s$
$t_v = 10s$
counts
times, s
(c)
XPS / Au 4f
$t_v = 1s$
$t_v = 10s$
Counts
time, s
(d)
QMS / amu 28
$t_v = 1s$
$t_v = 5s$
$t_v = 10s$
intensity, a.u.
time, s
(e)
N1s
QMS
$\Delta_t = 3(1)$
a.u.
t, s
(f)
TAPXPS
QMS
$m_0/max(m_0)$
t_v, s
(g)
$\overline{\tau_{res}} = 50(2.5)$
TAPXPS
QMS
$\tau_{res} = m_1/m_0, s$
t_v, s
(h)
Center
Area
FWHM

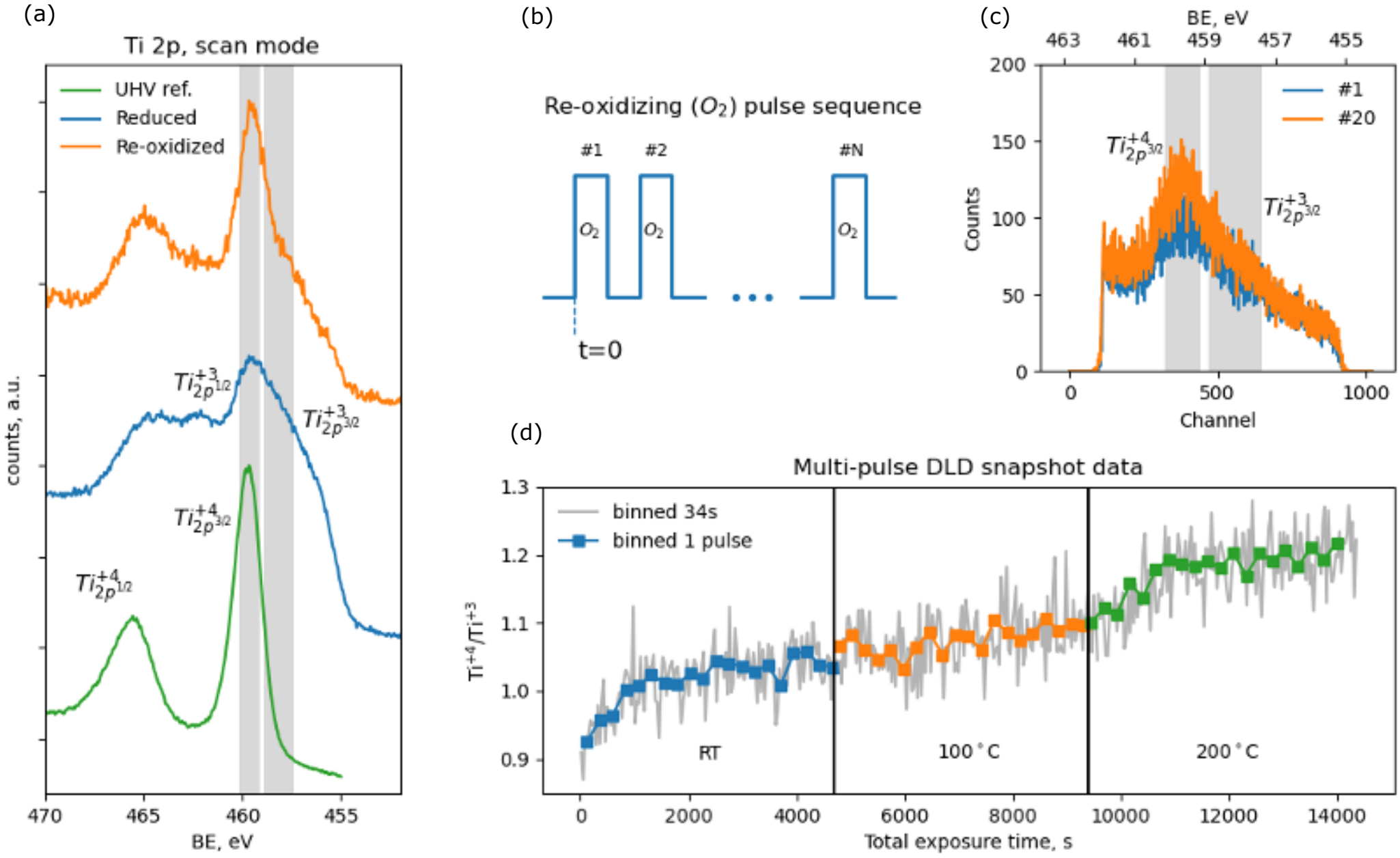
(a)
Ti 2p, scan mode
UHV ref.
Reduced
Re-oxidized
$Ti^{+3}_{2p^{1/2}}$
$Ti^{+3}_{2p^{3/2}}$
$Ti^{+4}_{2p^{3/2}}$
$Ti^{+4}_{2p^{1/2}}$
counts, a.u.
470
465
460
455
BE, eV
(b)
Re-oxidizing (O_2) pulse sequence
#1
#2
#N
O_2
O_2
O_2
t=0
(c)
BE, eV
463
461
459
457
455
200
150
100
50
0
Counts
#1
#20
$Ti^{+4}_{2p^{3/2}}$
$Ti^{+3}_{2p^{3/2}}$
0
500
1000
Channel
(d)
Multi-pulse DLD snapshot data
binned 34s
binned 1 pulse
1.3
1.2
1.1
1.0
0.9
Ti^{+4}/Ti^{+3}
RT
100 °C
200 °C
0
2000
4000
6000
8000
10000
12000
14000
Total exposure time, s

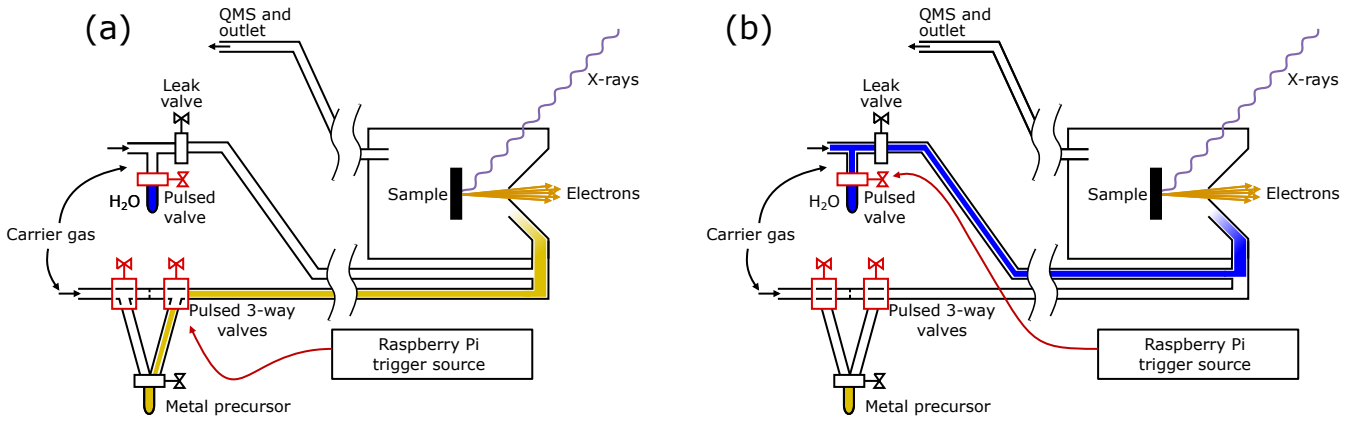
(a)
QMS and outlet
Leak valve
X-rays
H_2O
Pulsed valve
Sample
Electrons
Carrier gas
Pulsed 3-way valves
Raspberry Pi trigger source
Metal precursor
(b)
QMS and outlet
Leak valve
X-rays
H_2O
Pulsed valve
Sample
Electrons
Carrier gas
Pulsed 3-way valves
Raspberry Pi trigger source
Metal precursor

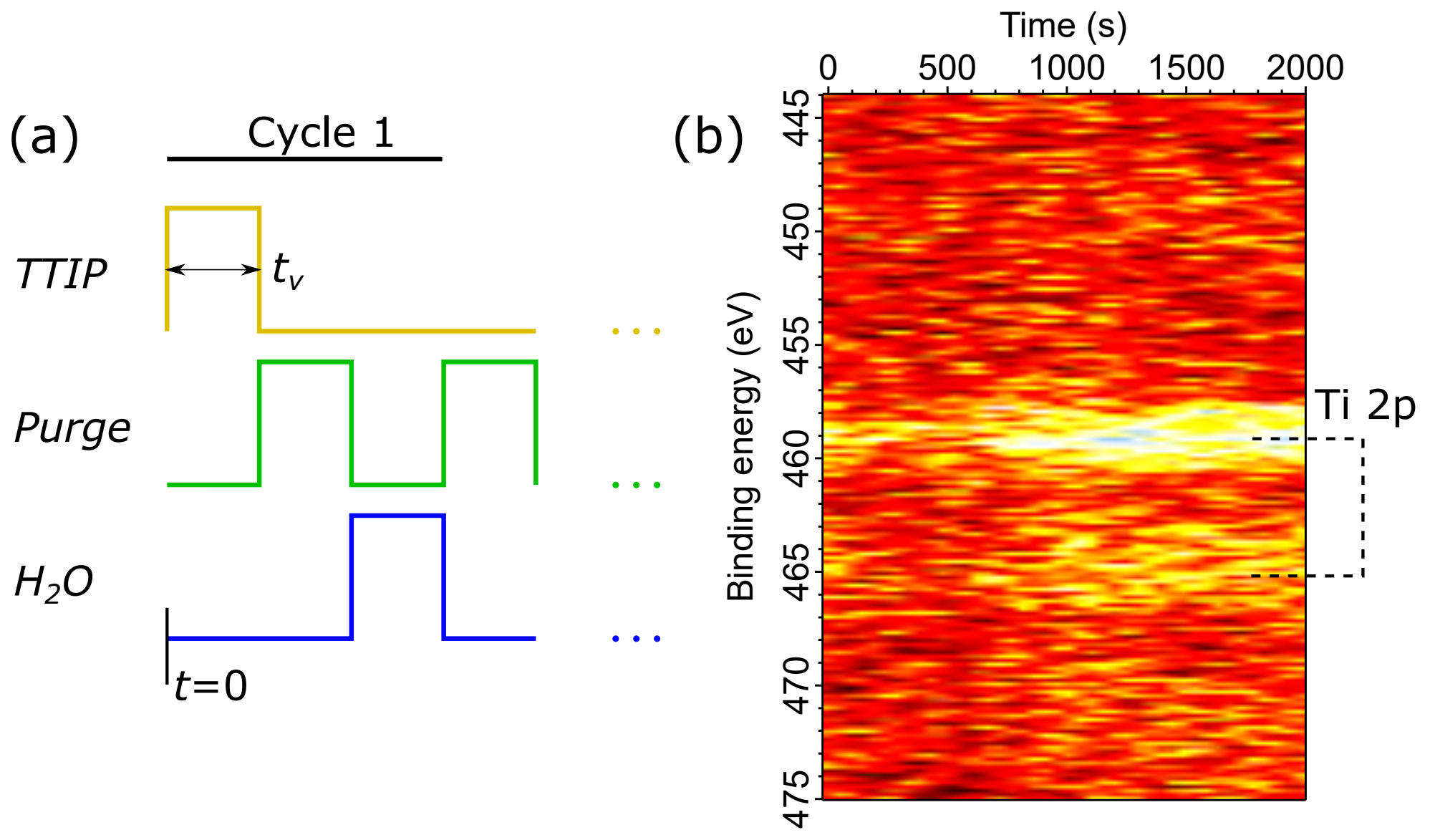
(a)
Cycle 1
TTIP
t_v
Purge
H_2O
t=0
(b)
Time (s)
0
500
1000
1500
2000
Binding energy (eV)
445
450
455
460
465
470
475
Ti 2p